Calibration of a wideband linear array

Pierre Cervenka, Jacques Marchal

10ème Congrès Français d'Acoustique

Lyon, 12-16 Avril 2010

Calibration of a wideband linear array

Pierre Cervenka[1,2], Jacques Marchal[2,1]

[1]CNRS, UMR 7190, Institut Jean le Rond d'Alembert, F-78210 Saint-Cyr-l'Ecole, France, pierre.cervenka@upmc.fr

[2]UPMC Univ. Paris 06, UMR 7190, Institut Jean le Rond d'Alembert, F-78210 Saint-Cyr-l'Ecole, France, jacques.marchal@upmc.fr

The bounded geometry of the experimental setup used to measure the directivity and sensitivity of array elements may raise several difficulties. In order to obtain the frequency response of wideband elements, the most straightforward method would be to transmit short pulses, and then to derive the transfer functions by applying Fourier transforms to the received signals. Unfortunately this approach often leads to poor signal-to-noise ratios within each frequency band because the amplitude of the transmitted pulse is limited. The usual solution consists of measuring the frequency responses by means of successive harmonic pings. However, the duration of such signals is also limited because of the possible interference between the waves following the direct path and those occurring from reflection with the tank envelope. The delays between the times of arrival are as much shorter as the distance between the source and the array to be calibrated is large. On the other hand, this distance must be sufficient to have an acoustic field that is uniform in the receiving area, and also to limit the parallax effect. The balance between these competing parameters leads to configurations where the direct signal and the first specular echo are as close as possible before overlapping. In order to properly derive the transfer functions, it is therefore mandatory to be able to delineate precisely the boundaries of the signals received from the direct path. We present here a reliable method for tracking these signals.

1 Introduction

In the underwater acoustic domain, the determination of the directivity and sensitivity of array elements over a relatively large frequency bandwidth may raise practical difficulties associated with the geometry of the experimental setup. We consider here the characterization of a receiving antenna by using a small source, but the reciprocal problem consisting of the characterization of a transmitting array by using a hydrophone at receive is equivalent.

In order to determine frequency transfer functions, a straightforward method consists of transmitting short, wideband pulses, and processing the received signals with the Fourier transform technique. However the amplitude of the transmitted signal being limited, this approach is often not suitable because leading to low signal-to-noise ratios in each frequency band. To get around this problem, the solution consists of making a series of measurements with narrow band quasi-harmonic signals, browsing the whole frequency range with successive pings. This method does not exclude to apply eventually narrower band-pass filters at post-processing, but the energetic content within each elementary band remains anyhow much larger than with the pulse method.

The narrower is the transmitted frequency band, the larger is the signal-to-noise ratio, but also the larger is the signal duration. Given the distance between the transmitter and the receiving array, there is a minimum delay between the waves that fly the direct path and the waves that are reflected by the envelope of the tank (most often, the geometry is such that the first mirror of concern is the free surface). In order to avoid the emergence of interferences, this delay dictates the maximal duration of the signals that can be used. The larger is the distance between the source and the array, the shorter is the available delay. Yet this distance must be sufficient for the acoustic field to be uniform enough around the array (farfield requirement), and also to a lesser extent for limiting the parallax. The balance between these competing parameters leads to settings such that the direct signal is close to overlap the first mirror echo. On the other hand, it is mandatory to process the entire received signals occurring from the direct path in order to derive properly the transfer functions. The practical problem consists of outlining with accuracy the limits of these direct signals without encroaching on the mirrored signals. Note that when measuring the angular characteristics of the elements in the plane that contains the array, the time of flight varies with the orientation of the array much more than the signals durations.

We present here a method that is reliable to track the exact positions of the direct signals in the records. The trick consists of using a set of signals at the different frequencies that are all centred in phase. At the post-processing stage, for each element and given the orientation of the array, the coherent sums of all the signals received at the different frequencies are computed. The envelope of these sums exhibits a narrow peak which is easy to detect. The positions of these maxima provide a set of arrival delays. The accuracy of these delays can be furthermore improved by fitting the estimates with a model based on the geometry of the setup. This process is described with an experimental example.

2 Experimental setup

2.1 Geometry

The task consists of measuring the sensitivity and directivity of the elements of a receiving linear array. The frequency range is 80 kHz – 130 kHz. The total length of the antenna is $L \approx 1.9$ m. There are 64 elements, with a pitch $\Delta u = 29.5$ mm. The actual size of the active face of each element is $l_a = 28$ mm × $l_b = 7$ mm.

The measurements are carried out in a large tank (B16) which is part of the naval facilities in Brest. The dimensions of the tank are: 80 m length, 10 m width, 8.4 m water column height (figure 1).

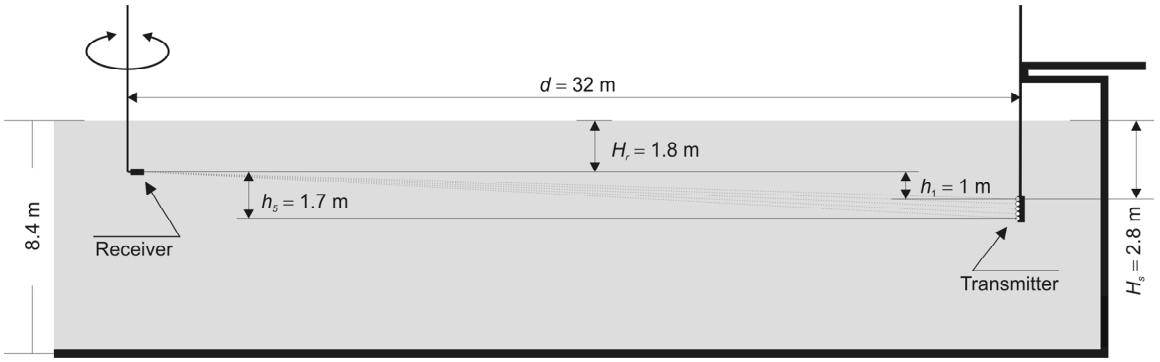

Figure 1: Longitudinal section of the tank – Layout of the elements (horizontal arrangement of the receiving antenna).

The sources are elements of another array (48 channels). This antenna is hung vertically, at the middle of one end of the tank. The upper side of this antenna is located at $H_s \approx 2.80$ m depth under the surface. A single channel is active during each ping. The only channels #1, #12, #24, #36 and #48 (numbering increasing downwards) are used as sources. The geometrical distribution of these sources within the array is displayed in Table 1.

Source (j)	1	2	3	4	5
Channel	#1	#12	#24	#36	#48
Δh_j (cm)	0	16.4	34.0	52.9	70.5

Table 1: Relative location of sources S_j in the transmitting array (S_1 as reference).

The receiving antenna is deployed from a deck across the tank. The distance from the source is $d \approx 32$ m. The suspension of the antenna includes a vertical axis of rotation. The mobile carriage that supports this axis is adjusted laterally on the deck so that the receiving antenna is located as much as possible at boresight of the sources. Two distinct configurations have been used to fasten the receiving antenna to the axis: horizontal and vertical positioning of the array. In order to illustrate the presented method, the only horizontal configuration is addressed here (figures 1 and 2). With this setting, the directivities of the elements are measured in the principal plane that contains the array. A hydrophone is also arranged for reference purpose a few decimetres above the array, close to its centre.

One considers two left-hand reference frames. One frame is still; the second one is attached to the receiving antenna. The axis of rotation defines the z-axis that is common for both frames, pointing downwards. The antenna is assumed to be properly mounted perpendicularly to this axis. The origin is also the same for both frames. It is chosen so that the z-coordinates of all the array elements are null. It is also assumed that the sources are properly aligned vertically, i.e. parallel to the z-axis. The direction between this axis and the sources defines the y-axis of the fixed frame.

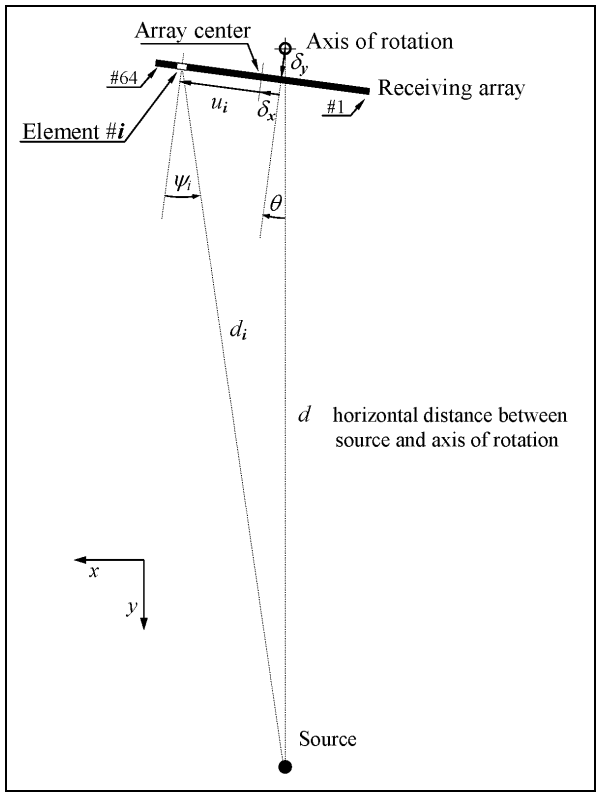

Figure 2: Measurement in azimuth (top view).
In this figure, $u_i > 0$, $\theta < 0°$ and $\psi_i > 0$. Note that the angle of view $|\psi_i|$ differs from the array orientation $|\theta|$.

Because of the limited length of the connecting cable, the receiving antenna could not be immersed at a depth larger than $H_r = 1.8$ m. The altitude difference between the array and the shallowest source is thus $h_0 = H_r - H_s \approx 1$ m. The coordinates of the sources S_j read

$$\mathbf{S}_j = \begin{bmatrix} 0 \\ d \\ h_j = h_0 + \Delta h_j \end{bmatrix}, \qquad (1)$$

where Δh_j are given in table 1.

The antenna frame makes an angle θ with the fixed frame ($\theta < 0$ in figure 2). The array is not exactly centred on the rotation axis: (δ_x, δ_y) denote the coordinates of the array centre in the antenna frame. The abscissa of element #*i*, referenced to the array centre, is denoted u_i. Hence the coordinates of element #*i* read in the fixed frame:

$$\begin{bmatrix} x_i \\ y_i \\ z_i \end{bmatrix} = \begin{bmatrix} \cos\theta & -\sin\theta & 0 \\ \sin\theta & \cos\theta & 0 \\ 0 & 0 & 1 \end{bmatrix} \begin{bmatrix} \delta_x + u_i \\ \delta_y \\ 0 \end{bmatrix} \quad (2)$$

with $u_i = (i - 32.5)\Delta u$ and $i = 1 \ldots 64$.

The orientation of the antenna is marked by means of a telemetry system. There is no absolute zero offset (manual setting). The difference between the indexed angle ϕ and the actual orientation θ is denoted δ_θ. During the measurement, a symmetrical 120° wide sector is swept with a pitch of $\Delta\theta = 2°$. Hence, there are 61 scanned positions that correspond to the following actual orientations θ_n:

$$\theta_n = \phi_n - \delta_\theta , \quad (3)$$

with $\phi_n = -60° + (n-1)\Delta\theta$ and $n = 1,\ldots,61$.

It must be noticed that for practical reasons, the parameters δ_θ, δ_x, δ_y, h_0 and d are not accurately known. On the other hand, the parameters ϕ_n, Δh_j and u_i are well defined.

2.2 Parallax

Although the distance d is significantly larger than the array length L ($0.5\,L / d \approx 1/16$), the bias that is introduced by the parallax must be taken into account for in determining the directivity pattern of each element #*i*: the difference between the inverse $-\theta$ of the antenna orientation and the actual angle ψ_i from which each element #*i* views the sources is not negligible:

$$\tan\psi_i = \frac{u_i + \delta_x - d\sin\theta}{d\cos\theta - \delta_y} , \quad (4)$$

so that

$$\begin{aligned} \Delta\theta_i &= \psi_i + \theta \\ &= \arctan \frac{(u_i + \delta_x)\cos\theta - \delta_y \sin\theta}{d - (u_i + \delta_x)\sin\theta - \delta_y \cos\theta} \\ &\approx \frac{(u_i + \delta_x)\cos\theta - \delta_y \sin\theta}{d} \end{aligned} \quad (5)$$

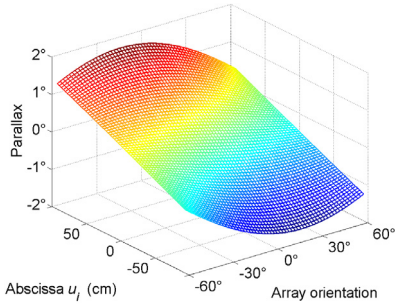

Figure 3. Parallax angle.

The latter approximation is obtained by taken into account that d is much larger than δ_x, δ_y and u_i. Figure 3 displays the parallax angles $\Delta\theta_i$. It can be checked that this angle can be as large as 2°, i.e. equal to the angular sampling pitch.

2.3 Distance sources-elements

The orientation of the array being θ, the distance $r_j(u,\theta)$ between the source S_j and an element whose relative abscissa is u reads:

$$r_j(u,\theta) = \sqrt{(d\cos\theta - \delta_y)^2 + (u + \delta_x - d\sin\theta)^2 + h_j^2} . \quad (6)$$

Because these distances are much larger than the lateral dimension of the array, the Fresnel approximation holds. It allows developing the distances r as a quadratic form in u:

$$r_j(u,\theta) \approx a_{j,\theta} u^2 + b_{j,\theta} u + c_{j,\theta} . \quad (7)$$

The abscissas u_i and the parameters δ_x, δ_y and h_j are altogether much smaller than the distance d, so that the development given in (6) can be made explicit according to:

$$\begin{aligned} r_j(u,\theta) \approx d &- (\delta_y \cos\theta + (u + \delta_x)\sin\theta) \\ &+ \frac{(\delta_y \sin\theta - (u + \delta_x)\cos\theta)^2 + h_j^2}{2d} \end{aligned} \quad (8)$$

The coefficients a, b et c can be then derived by equating each term in (7) with (8):

$$\begin{cases} a = \dfrac{\cos^2\theta}{2d} \\ b = -\sin\theta + \dfrac{\delta_x \cos\theta - \delta_y \sin\theta}{d}\cos\theta \\ c = d - (\delta_x \sin\theta + \delta_y \cos\theta) \\ \qquad + \dfrac{(\delta_x \cos\theta - \delta_y \sin\theta)^2 + h_j^2}{2d} \end{cases} \quad (9)$$

By the way, it can be noticed in the latter formulation that the coefficients a and b are the same for all sources, and that they depend only on the orientation θ of the array ($a_{j,\theta} = a_\theta$ and $b_{j,\theta} = b_\theta$). Coefficient a accounts for the curvature of the wave front. Coefficient b is mainly dictated by the steering angle. Coefficient c is a close approximation of the distance between the sources and the centre of the receiving array.

2.4 Delay between direct path and surface reflection

The receiving elements #*i* and the sources S_j are located at depth H_r and $(H_r + h_j)$, respectively. From (2), the horizontal distance $d_{i,\theta}$ between them reads:

$$\begin{aligned} d_{i,\theta}^2 = d^2 &+ (\delta_x + u_i)^2 + \delta_y^2 \\ &- 2d\left((\delta_x + u_i)\sin\theta + \delta_y \cos\theta\right) \end{aligned} , \quad (10)$$

and the travel difference $\Delta r_{i,\theta j}$ between the direct path and the indirect path after reflection on the free surface is:

$$\Delta r_{i,\theta,j} = \sqrt{d_{i,\theta}^2 + \left(2H_r + h_j\right)^2} - \sqrt{d_{i,\theta}^2 + h_j^2} \approx 2d^{-1}H_r\left(H_r + h_j\right) \qquad \left(d \gg H, h_j\right) \tag{11}$$

The shortest differences occur with the closest source from the surface (S_1). Considering the central area of the receiving antenna, when steered toward the source ($\theta = 0$), there is the following order of magnitude ($H_r \approx 1.8$ m, $d \approx 32$ m et $h_1 \approx 1$ m):

$$\Delta r \approx 2d^{-1}H\left(H + h_1\right) \approx 20 \text{ cm} \equiv \Delta t \approx 220 \text{ µs}. \tag{12}$$

This delay corresponds to less than 18 periods at frequency 80 kHz, i.e. the lower bound of the bandwidth of interest. This small margin is furthermore reduced because of the enlargement that the transfer functions, both at transmit and at receive, induce in the recorded signals. On the other hand, the distances between the sources and most of the receiving elements vary much more that the delay given in (12) during the rotation of the antenna. It implies that a rigorous determination of the measuring windows is called for in such a configuration.

3 Processing scheme

3.1 Signals

The discrimination between the signals coming from the direct path and from the surface reflection would not be a problem if a short, wideband signal was issued at transmit. Unfortunately, using such a pulse would result in a poor signal-to-noise ratio.

Loosely said, an infinite sum of equal amplitude sinusoids covering all frequencies with the proper phasing is equivalent to a Dirac distribution. Less drastically, the sum of a finite number of sinusoids spanning a finite bandwidth, when properly phased, results in a sharp shaped function. One takes advantage of this simple evidence to track accurately the limits of harmonic signals received by the elements to be calibrated.

At each ping, a 12-periods sinus signal is fed to a source. For each orientation of the antenna, a collection of 51 such signals is sequentially transmitted, spanning the 80 kHz – 130 kHz frequency range with a 1 kHz pitch:

$$s_\nu(t) = -\text{rect}\left(n_s/\nu\right)\sin\left(2\pi\nu t\right), \quad \nu = k\nu_0, \tag{13}$$

$$\nu_0 = 1 \text{ kHz} \quad \text{and} \quad k = 80:130, \quad n_s = 12.$$

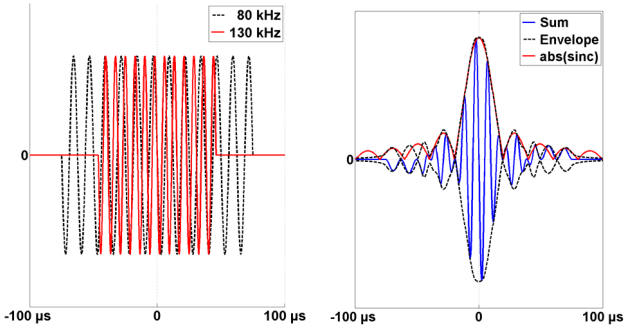

Figure 4: Left: examples of signals used to drive the sources; Right: sum of the signals depicted by (13) (blue line); envelope of this sum (dashed line); approximation with a cardinal sinus (red line) - see (15).

Notice that these signals are all centred with a null value in the transmit window (see for examples figure 4 - left).

The coherent sum of the central part (i.e. without any truncation) of these signals reads:

$$S\left(|t| < 46 \text{ µs}\right) = \sum_\nu s_\nu = -\frac{\sin\left(\pi\left(k_{\max} - k_{\min} + 1\right)\nu_0 t\right)\sin\left(\pi\left(k_{\max} + k_{\min}\right)\nu_0 t\right)}{\sin\left(\pi\nu_0 t\right)} \qquad \left(k_{\min} = 80, \quad k_{\max} = 130\right) \tag{14}$$

Because there is $|t| \ll \nu_0^{-1}$ (≈ 1 ms) in the time domain of interest, (14) can be approximated with:

$$S \cong -\left(k_{\max} - k_{\min}\right)\sin\left(\pi\left(k_{\max} + k_{\min}\right)\nu_0 t\right) \times \text{sinc}\left(\pi\left(k_{\max} - k_{\min}\right)\nu_0 t\right) \tag{15}$$

Hence, the envelope of the coherent sum of the synthesized signals is close to a cardinal sinus in its central part (figure 4 - right). The order of magnitude of the peak width is dictated by the total bandwidth, i.e. $(k_{\max} - k_{\min})\ \nu_0 = 50$ kHz:

$$\Delta t \equiv 2\left(\left(k_{\max} - k_{\min}\right)\nu_0\right)^{-1} \approx 40\mu s. \tag{16}$$

This value is significantly smaller than the duration of the shortest synthesized signal ($T_{130\text{kHz}} = 92$ µs). Moreover, this peak width is much smaller than the 220 µs estimated delay between the arrivals of the direct signal and of the surface reflection (see (12)). Hence, there is no risk to make any confusion with the peak associated with the indirect path. This technique has another interest when the orientation of the antenna corresponds to the sector between the main lobe and the first side lobe. Given an angle of view, the frequency bandwidth is large enough so that vanishing levels is of concern for a limited part of the band: the envelope of the sum features always a maxima that can be properly detected.

3.2 Initial search for wave fronts

In the presented experiment, the number of transmit cycles is therefore equal to 15,555 pings (5 sources × 51 frequencies × 61 angles), which produces 995,520 recorded signals $s_{i,j,\theta,\omega}(t)$ (64 elements). The index j is dropped in the remaining part of this section as the sets of data obtained with the different sources are processed independently of each other.

The first step in the data processing consists of computing the sums

$$E_{i,\theta}(t) = \left|\text{TH}\left(\sum_\omega s_{i,\theta,\omega}\right)\right|, \tag{17}$$

where TH denotes the Hilbert transform (the continuous component that the signals may possibly contain is removed beforehand). The upper part of figure 5 exhibits the envelopes obtained with Source #1, at a few orientation angles. The wave-front corresponding to the direct path followed by the first multiple reflected by the free surface are clearly delineated. The algorithm that detects the instants of arrival is designed to scrutinize successively the

different orientations of the array. The process is initialized by hand with an estimate of the delays $\tilde{t}_{i,\theta_1}$ at the starting position $\phi_1 = -60°$. For any given orientation ϕ_n, the location t_{i,θ_n} of the maximum value of the envelope is searched for each element #i within a window ΔT that is centred on the initial seed.

$$E_{i,\theta_n}\left(t_{i,\theta_n}\right) = \max\left(E_{i,\theta_n}\left(t \in \left[\tilde{t}_{i,\theta_n} - \frac{\Delta T}{2}, \tilde{t}_{i,\theta_n} + \frac{\Delta T}{2}\right]\right)\right). \quad (18)$$

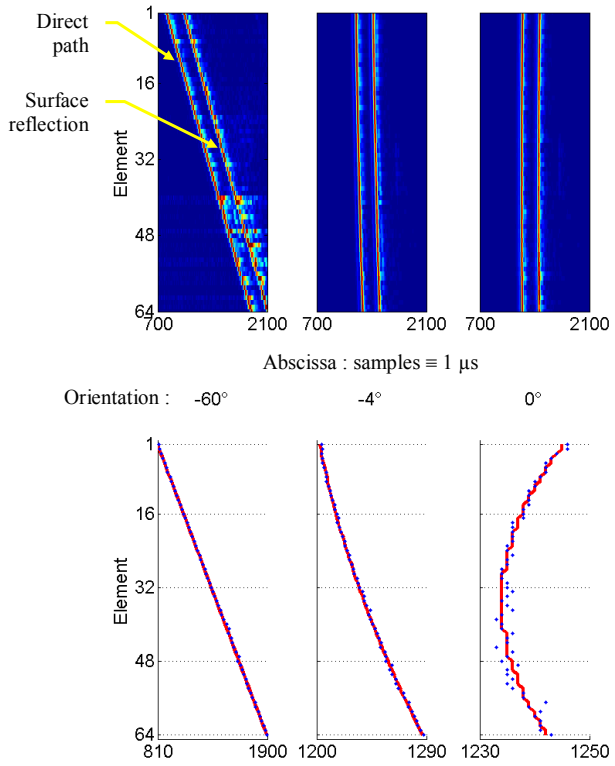

Figure 5: Up: envelope of the sum of the signals received at all frequencies (each horizontal line normalized with maximal value). Down: location of maxima (blue dots) and polynomial fitting (red line).

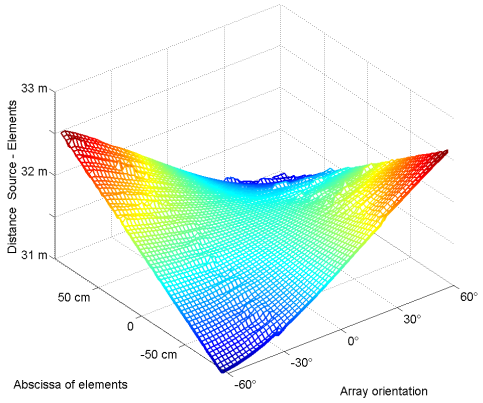

Figure 6: Distance between receiving elements and sources (blue dots in figure 5). Superimposed layers corresponding to 5 sources.

A least square fitting in the form given in (7) is performed on the resulting delays t_i. The smoothed delays $\tilde{t}_{i,\theta_n}$ are used as seeds to centre the windows in the next search iteration n+1. The width of the search window ($\Delta T = 100$ µs) is chosen so as to be large enough to support the shift in the arrival time between two adjacent orientation angles (23 µs with a 1 m arm level and a $\Delta\theta = 2°$ angular interval). On the other hand, ΔT is small enough, i.e. less than Δt (see (12)), so that there is no risk to catch the second wave-front.

Figure 6 displays the set of distances between the sources and the elements that are eventually found. But for the initial smoothed seeds determined at the previous iteration to centre the detection windows, each value r is obtained independently of each other, within the limits of the windows size. Although this process is robust enough to identify the signals occurring from the direct path, fluctuations that the geometry of the setup cannot account for can be noticed. Such fluctuations can induce an incorrect adjustment of the windows that are eventually used to crop the records before computing the received levels. The quality of this adjustment is critical because the size of the windows must be as large as possible, although not encroaching upon the second wave fronts. Hence, the source-elements distances that are actually used are computed with (6) from the model described in the previous section 2.3. However, several parameters in this geometrical model are not known with accuracy.

3.3 Direct model fitting

These values (δ_θ, δ_x, δ_y, h_0 and d) are derived by processing the first estimates of the distances with a classical least square fitting method. The model is given by (6). The data $r_{\text{experiment}}$ are the raw results displayed figure 6, i.e. without any smoothing process (blue dots in figure 5). The minimization process reads:

$$\frac{\partial}{\partial p}\left(C^2\right) = 0 \text{ with } C^2 = \sum_{u_i, S_j, \theta} \left(r_{\text{experimental}} - r_{\text{model}}\right)^2, \quad (19)$$

where $p = \delta_\theta, \delta_x, \delta_y$ or h_0.

Implemented as an iterative process, the parameter d is corrected at each step so as to keep null the mean difference between the data and the model:

$$\delta d = \left\langle r_{\text{experimental}} - r_{\text{model}} \right\rangle_{u_i, S_j, \theta}. \quad (20)$$

The convergence yields:

$$\delta_\theta = -0.20°, \ \delta_x = 15 \text{ mm}, \ \delta_y = 319 \text{ mm}, \\ h_0 = 1.01 \text{ m and } d = 31.871 \text{ m}. \quad (21)$$

The differences Δr between the final model and the raw data are displays figure 7. The standard deviation C is around 10 mm, i.e. the same order of magnitude as the wavelength, which is not negligible taking into account that the signal length is only 12λ. It can be also observed that the largest differences occur around 30° on both sides of the main axis. These directions correspond to the transition areas between the main lobe and the first side lobe of the elementary directivity patterns (the theoretical transition occurs at $|\theta| = \text{asin}(\lambda/l)$, e.g. $|\theta| = 32°$ at 100 kHz with $l_a = 28$ mm).

Notice that all the geometric parameters are counted with the natural dimension, i.e. length. Actually, the model is based on time measurements, and then converted as

distances through the proportionality relation with the celerity (1490 m/s in the sea water at the ambient temperature). The relative accuracy of this parameter is at best about 1/1000. Displaying the value of d in millimetres is therefore not significant in terms of the actual, absolute accuracy on this parameter.

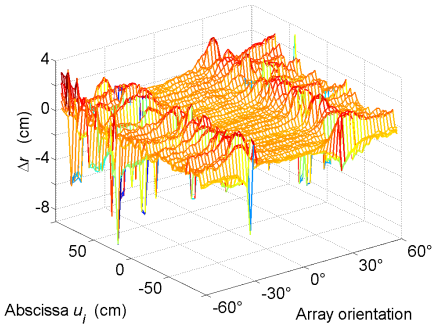

Figure 7. Difference between first estimates and model.

3.4 Results

The process described in the previous section yields delays $t_{0\,i,j,\theta} = d_{i,j,\theta}/c$ that correspond approximately to the middle of the signals received by the element #i (sent by the source S_j), the orientation of the antenna being θ. Given a particular frequency, the beginning of the reception can be retrieved by subtracting 2 contributions: the half duration of the synthesized signal; another small contribution that takes into account the signal spreading caused by the angle between the incoming wave front and the element face whose length is l_a:

$$t_{\text{init}\,i,j,\omega,\theta} = t_{0\,i,j,\theta} - \left(n\frac{2\pi}{\omega} + \frac{l_a}{c}\sin|\theta| \right) \Big/ 2 , \qquad (22)$$

where $n = 12$, $l_a = 28$ mm and $c = 1490$ m/s.

The windows must not encroach on the surface echoes. Consequently, the upper limits t_{end} are defined with (11):

$$t_{\text{end}\,i,j,\omega,\theta} = t_{\text{init}\,i,j,\omega,\theta} - \Delta r_{i,\theta,j}/c . \qquad (23)$$

The windows are slightly shifted back in order to preserve a small safety margin δt:

$$w_{i,j,\omega,\theta}(t) = \text{rect}\left(\frac{t - \frac{t_{\text{init}} + t_{\text{end}}}{2} + \delta t}{t_{\text{end}} - t_{\text{init}}} \right) . \qquad (24)$$

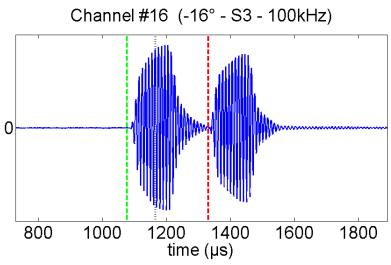

Figure 8. Example of a record and the estimated limits.

The frequency and angular elementary responses are computed with the only contribution of the central frequencies of the synthesized signals. Hence, the following integral is computed for each received signal $s_{i,j,\omega,\theta}$:

$$A_{i,j}(\omega,\theta) = \int w_{i,j,\omega,\theta}(t)\, H_{i,j,\omega,\theta}(t) \exp(-j\omega t)\,\mathrm{d}t , \qquad (25)$$

where H denotes the Hilbert transform of s (figure 8).

The signals received by the hydrophone that is located close to the receiving array centre undergo a process that is similar to (25), but for the dependency with the angle θ which is here meaningless.

$$A_{\text{hydro},j}(\omega) = \int w_{\text{hydro},j,\omega}(t)\, H_{\text{hydro},j,\omega}(t) \exp(-j\omega t)\,\mathrm{d}t . \qquad (26)$$

Knowing the sensitivity at receive $\text{SH}(\omega)$ of the hydrophone, the angular and frequency response of each array element can be derived with

$$\text{SH}_i(\omega, \psi = \Delta\theta_i - \theta) = 20\log_{10}\left\langle \frac{A_{i,j}(\omega,\theta)}{A_{\text{hydro},j}(\omega)} \right\rangle_j + \text{SH}_{\text{hydro}}(\omega) \qquad (27)$$

where the average of the results obtained with the 5 sources is performed. Such response is classically split in the on-axis sensitivity $\text{SH}_i(\omega)$ and the directivity $D_i(\omega, \psi)$:

$$\text{SH}_i(\omega,\psi) = \text{SH}_i(\omega) + \text{D}_i(\omega,\psi) , \qquad (28)$$

with $\text{D}_i(\omega, 0°) = 0$ dB. From a practical point of view, the arrays derived from (27) must be re-sampled to obtain an angular basis that is common for all elements. This is especially needed to recover the on-axis sensitivity $\text{SH}_i(\omega) = \text{SH}_i(\omega, \psi = 0°)$. The only mean response of the elements $\langle \text{SH}_i(\omega,\psi) \rangle_i$ is presented here (Figure 9).

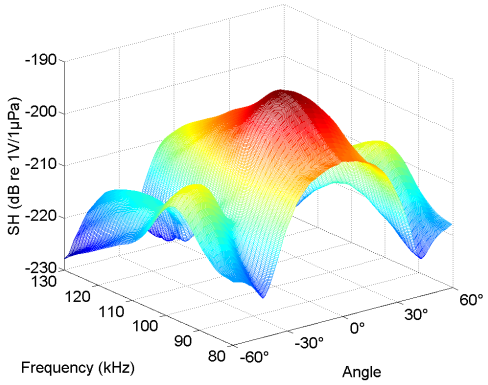

Figure 9: Mean response of the array elements.

4 Conclusion

The proposed method for tracking properly the received signals in a calibration process is simple to implement, provided the transmitted signals can be properly synthesized.

In addition, a fitting of the obtained delays with a model based on the geometry of the setup enables to retrieve several ill-known offsets (e.g. mounting shifts and angles). It leads to furthermore improve the accuracy of the received signals tracking.

Note that the determination of the missing parameters could be also performed by implementing a sophisticated high resolution based method, but at the expense of complexity which is not worth the specific, initial purpose.